

# *In Silico* Modelling of Transdermal and Systemic Kinetics of Topically Applied Solutes: Model Development and Initial Validation for Transdermal Nicotine

Tao Chen<sup>1</sup>  · Guoping Lian<sup>1,2</sup> · Panayiotis Kattou<sup>1</sup>

Received: 11 December 2015 / Accepted: 2 March 2016 / Published online: 8 March 2016  
© Springer Science+Business Media New York 2016

## ABSTRACT

**Purpose** The purpose was to develop a mechanistic mathematical model for predicting the pharmacokinetics of topically applied solutes penetrating through the skin and into the blood circulation. The model could be used to support the design of transdermal drug delivery systems and skin care products, and risk assessment of occupational or consumer exposure.

**Methods** A recently reported skin penetration model [Pharm Res 32 (2015) 1779] was integrated with the kinetic equations for dermis-to-capillary transport and systemic circulation. All model parameters were determined separately from the molecular, microscopic and physiological bases, without fitting to the *in vivo* data to be predicted. Published clinical studies of nicotine were used for model demonstration.

**Results** The predicted plasma kinetics is in good agreement with observed clinical data. The simulated two-dimensional concentration profile in the stratum corneum vividly illustrates the local sub-cellular disposition kinetics, including tortuous lipid pathway for diffusion and the “reservoir” effect of the corneocytes.

**Conclusions** A mechanistic model for predicting transdermal and systemic kinetics was developed and demonstrated with published clinical data. The integrated mechanistic approach has significantly extended the applicability of a recently reported microscopic skin penetration model by providing prediction of solute concentration in the blood.

**KEY WORDS** diffusion · disposition · percutaneous absorption · physiologically-based pharmacokinetic modelling · toxicokinetics

## ABBREVIATIONS

3Rs	Replacement refinement and reduction
CVODE	C-language variable-coefficients ODE solver
MW	Molecular weight
ODE	Ordinary differential equation
PDE	Partial differential equation
QSPR	Quantitative structure–property relationship
SUNDIALS	SUite of nonlinear and differential/algebraic equation solvers
SWIG	Simplified wrapper and interface generator

## INTRODUCTION

Transdermal permeation of chemicals is an important topic in a range of applications, such as transdermal delivery of drugs, design of skin care and cosmetic products, and safety assurance and risk assessment of exposure to hazardous chemicals. Due to its effective barrier properties, skin is of significant interest to controlled release of pharmaceutical and other products (1, 2). In the past, research in this field largely relied on *in vivo*, *ex vivo* and *in vitro* tests (especially in early phase development), and clinical studies with human volunteers (typically in late phase trials). This empirical approach is time consuming and expensive. In recent years, the research paradigm has undergone a significant change towards more mechanistic and holistic understanding of various transdermal permeation pathways, including the role of the physico-chemical properties of the solute of interest and its interaction with skin. Within this context, mathematical modelling, also referred to as *in silico* approach, has emerged as an important technology to improve fundamental understanding of the transdermal

✉ Tao Chen  
t.chen@surrey.ac.uk

<sup>1</sup> Department of Chemical and Process Engineering, University of Surrey, Guildford GU2 7XH, UK

<sup>2</sup> Unilever Research Colworth, Colworth Park, Sharnbrook, Bedfordshire MK44 1LQ, UK

permeation kinetics. This *in silico* approach is also an important approach to the replacement, refinement and reduction of animal tests in research (the 3Rs).

In the literature, various modelling studies on transdermal permeation have been reported. A frequently cited approach is the empirical quantitative structure–property relationship (QSPR) models, which intend to predict the steady-state permeability coefficient based on experimental results of percutaneous absorption (3, 4). Extension from steady-state to kinetic modelling has been achieved by the compartmental approach, which treats the skin layers as different compartments each having uniform concentration, *e.g.* (5, 6) and other studies reviewed by Anissimov *et al.* (7). A major limitation of the compartment model is that the model parameters often need to be fitted to experimental data, and thus the extrapolation capability is limited. More recently, significant attention has been given to the diffusion-based models that use the Fick's second law of diffusion to describe time-dependant solute diffusion across skin layers. Early diffusion-based models ignored the heterogeneous structure of the stratum corneum and described the transdermal permeation as diffusion in homogeneous media (8, 9); however the model parameters also needed to be fitted to experimental data in order to make satisfactory predictions. Since the heterogeneous “brick-and-mortar” structure of the stratum corneum was introduced to *in silico* modelling, the main challenge has been to obtain the transport and disposition properties (diffusion and partition coefficients). Some models chose to obtain these properties by data-fitting (10), limiting the applicability of the model. Wang *et al.* (11, 12) reported a more predictive two-dimensional model, in which the diffusion and partition coefficients were obtained from fundamental principles, and only the trans-bilayer mass transfer coefficient was fitted to deduce a correlation with the molecular weight. A similar two-dimensional approach was taken by Lian and co-workers (13, 14), where data-fitting was only used to derive a correlation for calculating the diffusion coefficient in corneocytes, and the prediction accuracy was significantly improved when compared with the Wang's model in (11, 12). With consideration of the two-dimensional microscopic skin structure, both models (11–14) demonstrated the importance of the trans-cellular diffusion pathway through the stratum corneum. In a later study, Lian and co-workers extended their model to include viable epidermis and dermis whilst maintaining the predictive capability (15). Some excellent review articles have been published to summarise the recent progress in this area; see *e.g.* (7, 16, 17).

The majority of the transdermal permeation models developed, especially those incorporating more realistic heterogeneous skin physiology (11–13, 15), were intended to predict the absorption kinetics in the skin only. When the chemical reaches the dermis, it is cleared from the skin through both diffusion into deeper tissues and convection by the capillary blood vessels. Although the dermis clearance pathways have

been modelled (18–21), the focus was still on improving the modelling accuracy within skin. The kinetics in systemic circulation has not been considered in these studies. Systemic circulation was included in many compartment-based pharmacokinetic models (5, 6, 22), but they have limited predictive capability due to the lack of sufficient microscopic details in skin. Therefore, there is a need to connect the microscopic skin penetration models with systemic circulation kinetics, so that prediction capability can be extended to the concentration profile in circulation. This capability is important because the plasma concentration profile is one of the primary parameters from the efficacy and safety perspectives in many applications. In addition, by validating the model against *in vivo* plasma data, one can also infer detailed kinetic and bioavailability information in various skin layers from the model, which are not normally available in clinical studies.

Against this background, this study aims to integrate our recently reported skin penetration model with systemic circulation kinetics. Following the previous studies (13, 15), the brick-and-mortar model is used to represent the heterogeneous structure of the stratum corneum, while the viable epidermis and dermis are modelled as homogenised material with properties related to the main compositions of cellular lipid, protein and water. The transport of chemicals within skin is governed by diffusion equations, and that into capillary blood is modelled by using the assumption of equilibrium between dermis and blood, following the method in (5). Importantly, the partition and diffusion properties are calculated by relating to the fundamental physico-chemical properties of solutes, rather than fitting to the data to be predicted. The physiology in skin and blood circulation (*e.g.* depth of skin layers, capillary blood flow rate, whole body blood volume, *etc.*) is also used. The model has been implemented in C++, which allowed fast computation using a much finer grid scheme in stratum corneum than reported previously (13, 15). It should be noted that the coarse grids previously used (13, 15) were deemed numerically sufficient for predicting one-dimensional pharmacokinetics, as further refinement of the grids did not improve the resolution. However, for the purpose of simulating detailed two-dimensional local disposition, higher resolution is needed and this is the motivation of using finer grids in the present study. The model is applied to predict the published data from clinical studies of transdermal nicotine patches (23, 24). The prediction is in good agreement with the published data, showing excellent prediction capability achieved with the integrated model of both transdermal permeation kinetics and systemic circulation kinetics. In addition, the simulated detailed two-dimensional concentration profile of nicotine in the stratum corneum vividly illustrates the tortuous lipid pathway for diffusion (the “fingering” effect) and the “reservoir” effect of the corneocytes.

## MATERIAL AND METHODS

This section describes the modelling method in general, followed by the particular details of reported clinical studies of nicotine that were used for the initial validation and demonstration of the model.

### The Mathematical Model

Figure 1 illustrates the modelling framework including a single homogenous vehicle layer, a two-dimensional heterogeneous brick-and-mortar structure of the stratum corneum, one-dimensional (vertical diffusion) schemes for the viable epidermis and dermis, the coupling of solute diffusion in dermis with transport into the blood capillaries, and the solute clearance in the circulation. The simulation scheme for stratum corneum, viable epidermis and dermis is the same as the previous study (15).

### The Overall Simulation Approach

The simulation is based on solving the diffusion equation that describes the transport of solute. The time- and space-dependent partial differential equation (PDE) of diffusion is solved by the method of lines. More specifically, the simulation domain is discretised into grids, which allow for the conversion of the PDE into a large number of ordinary differential equations (ODEs). The grid scheme for the vehicle (one grid), the viable epidermis (ten vertically and equally spaced grids) and the dermis (ten vertically and equally spaced grids) is the same as in the previous study (15). However, to allow for detailed simulation of the stratum corneum, the main

penetration barrier, much finer grids were used: in the vertical direction, two grids were used for the lipid bi-layer and four for the corneocytes; in the lateral direction, two grids were used for the inter-cellular lipid and 20 for the corneocytes. In total, this gives rise to 3189 grids in the skin, plus one compartment for the blood (*i.e.* 3190 ODEs).

The flux due to diffusion between any two neighbouring grids, either in the vertical or lateral direction, in the simulation domain is described by the following mass transfer equation:

$$q_{ij} = \frac{A}{\frac{\delta_i}{D_i} + \frac{K_{ij}\delta_j}{D_j}} (C_i - K_{ij}C_j) \quad (1)$$

where  $q_{ij}$  is the rate of mass transfer ( $\text{kg s}^{-1}$ ) from grid  $i$  to grid  $j$ ,  $A$  is the interfacial area between the two grids,  $\delta_i$  and  $\delta_j$  are the corresponding diffusion lengths,  $D_i$  and  $D_j$  are the diffusivity of the corresponding grids,  $K_{ij}$  is the solute partition coefficient between grid  $i$  and  $j$ , and  $C_i$  and  $C_j$  are the concentration in grid  $i$  and  $j$ , respectively. Since water is the reference used for partition coefficients,  $K_{ij}$  can be calculated as the ratio of  $K_{iw}$  (partition coefficient from grid  $i$  to water) to  $K_{jw}$  (partition coefficient from grid  $j$  to water), which depend on the type of material of the grid and the calculation will be detailed in Section 2.1.2.

Building on the mass transfer rate described in Eq. (1), the law of mass conservation requires that the concentration in each simulation grid in the vehicle, stratum corneum and viable epidermis follows the differential equation:

$$V_i \frac{dC_i}{dt} = - \sum_j q_{ij} \quad (2)$$

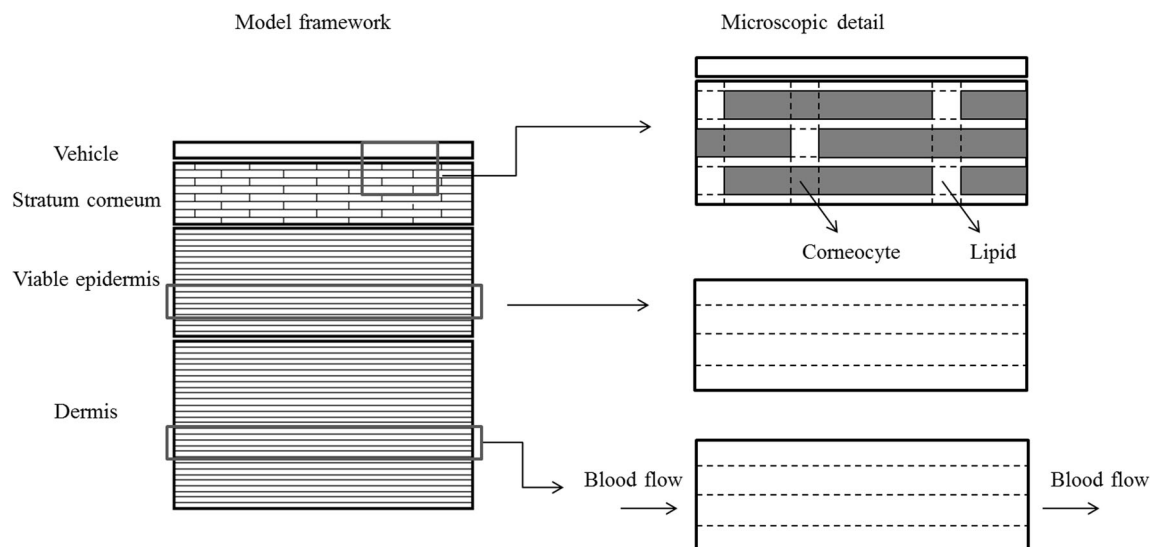


**Fig. 1** Overview of the modelling framework.

where  $V_i$  is the volume of grid  $i$ ,  $t$  is time, and the summation is for all the grids that are neighbours of grid  $i$ .

In addition to diffusion, convection needs to be considered when modelling the transport between dermis and capillaries due to the blood flow. We follow Bookout Jr *et al.* (5) to model each grid in the dermis as a homogeneous volume, and the solute in blood circulation has a uniform concentration. Based on these assumptions, within each dermis grid, the solute convection of the capillary into the grid is given by  $Q_{b,i}C_b$ , where  $Q_{b,i}$  is the blood flow into the dermis grid  $i$  and  $C_b$  is the solute concentration in the blood. When the capillary flow leaves the dermis grid, the capillary concentration is assumed to be in equilibrium with the concentration in the dermis grid, and thus the solute flux taken away by the capillary is given by  $Q_{b,i}C_i/K_{db}$ , where  $K_{db}$  is the partition coefficient from dermis to blood. Therefore, for a dermis grid  $i$ , the mass balance equation is

$$V_i \frac{dC_i}{dt} = - \sum_j q_{ij} + Q_{b,i} \left( C_b - \frac{C_i}{K_{db}} \right) \tag{3}$$

The above equilibrium assumption can be viewed as a simplification of the capillary clearance models reported in (18, 19), in which transient equations were used to model the permeation of solute from dermis into capillary. The transient equations are more complex since the permeability between dermis and capillary needs to be considered, in addition to the partition coefficient.

The volumetric blood flow,  $Q_{b,i}$ , can be estimated according to physiology. It is known that the average resting cardiac output is ca. 5.6 L min<sup>-1</sup> for a human male and 4.9 L min<sup>-1</sup> for a female (25), and the overall blood flow to skin is estimated to be 5% of cardiac output (5). Therefore, the overall skin blood flow can be estimated (0.05 × 5.6 = 0.28 L min<sup>-1</sup> for male and 0.05 × 4.9 = 0.245 L min<sup>-1</sup>). The blood flow is assumed to be distributed uniformly in the dermis; therefore the flow in each dermis grid ( $Q_{b,i}$ ) can be calculated based on the volume of the grid and the volume of the dermis. We used the average skin surface area (1.8 m<sup>2</sup>) and typical dermis thickness of 1.2 mm (15) to calculate the volume of the dermis, therefore the model represents the absorption kinetics of a typical person.

The systemic circulation and clearance is described by the following equation:

$$V_b \frac{dC_b}{dt} = \mathcal{N} \sum_i Q_{b,i} \left( \frac{C_i}{K_{db}} - C_b \right) - kC_b \tag{4}$$

where  $V_b$  is the volume of whole-body blood vessel, and  $kC_b$  is the first-order clearance that may include

transport into other tissues and metabolism. The summation is with respect to all dermis grids, and  $\mathcal{N}$  is the ratio of actual topical application area and the area being simulated. For computational efficiency, the lateral length being simulated usually covers a few corneocytes (one corneocyte in this study), and thus the simulated area is much smaller than the actual application area. The whole-body blood volume,  $V_b$ , can be calculated from the typical fraction of blood mass to that of adult body weight (7%) and the blood density (1.06 of water density). The clearance rate,  $k$ , of many pharmaceutically or toxicologically important chemicals is available from clinical pharmacokinetic studies of oral and/or intravenous delivery routes.

The simulation was performed by solving the ODEs on the grids explained above. All initial concentration is set to zero, except that in the vehicle. The left and right boundaries in the stratum corneum are periodic conditions, to represent a large application area.

The model was implemented in C++, where the differential equations are solved by calling the state-of-the-art CVODE solver as part of the SUNDIALS computational package (26) developed in the Lawrence Livermore National Laboratory (computation.llnl.gov/casc/sundials). The user interface was written in Python (www.python.org) with extensive use of Scipy (a scientific module of Python, www.scipy.org). Interfacing between C++ and Python was achieved by using the SWIG (Simplified Wrapper and Interface Generator, www.swig.org) tool. The hybrid programming method was useful to achieve sufficient computational efficiency when solving a large number (3190) of differential equations, whilst limiting the developmental time. The source code is publicly available at www.github.com/anthonytchen/lck. All computation was conducted on a laptop computer with dualcore CPU (2.80 GHz) installed with an Ubuntu (version 15.04) Linux operating system.

### Diffusion and Partition Coefficients of Skin and Vehicle

The diffusion and partition coefficients of skin and vehicle depend on the physicochemical properties of the solute, including the molecular weight (MW, Da), the hydrophobicity in terms of octanol/water partition coefficient ( $K_{ow}$ ), the dissociation constant (pKa), as well as the composition of the skin. A range of QSPR models have been reported for calculating the diffusion and partition parameters. In this section, the QSPR methods implemented in our model is outlined for completeness. More details can be found in the original articles (13, 15, 27).

In the vehicle, the diffusion and partition coefficients depend on the formulation. If a simple aqueous solution is used,

the partition coefficient between vehicle and water,  $K_{vw}$ , is unity, and the diffusion coefficient can be calculated using the Stokes-Einstein equation:

$$D_w = \frac{KT}{6\pi\eta r_s} \quad (5)$$

where  $K$  is the Boltzmann constant,  $T$  is the temperature,  $\eta$  is the viscosity of water and  $r_s$  is the solute radius (Å) calculated as:  $r_s = \sqrt[3]{3/4 \times 0.0987MW}$  (28).

In the stratum corneum, the partition coefficient between the “mortar” (the lipid bilayer) and water is determined by the following relationship:

$$K_{mw} = \frac{\rho_l K_{ow}^{0.69}}{\rho_w} \quad (6)$$

where  $\rho_l$  and  $\rho_w$  are the bulk density of lipid and water, respectively. The solute diffusion coefficient,  $D_m$  ( $\text{m}^2 \text{s}^{-1}$ ) in the lipid is related to solute radius as described in (1, 13):

$$D_m = \begin{cases} 2 \times 10^{-9} \exp(-0.46 r_s^2), & MW \leq 380Da \\ 3 \times 10^{-13}, & MW > 380Da \end{cases} \quad (7)$$

The partition coefficient between corneocytes (*i.e.* the “brick”) and water ( $K_{bw}$ ) is estimated from the volume fraction of water in corneocytes ( $\phi_b$  is the fraction at saturation and  $\theta_b$  is the actual fraction), and the solute binding constant to keratin in stratum corneum ( $K_{kw}$ ):

$$K_{bw} = (1 - \phi_b)K_{kw} + \theta_b \quad (8)$$

where  $K_{kw} = \rho_k/\rho_w \times 4.2K_{ow}^{0.31}$  and  $\rho_k$  is the bulk density of keratin (29, 30). The diffusion coefficient in the corneocyte ( $D_b$ ) is estimated according to the following equation of hindered diffusion (13):

$$D_b = \frac{\exp(-\alpha S^2)}{1 + \frac{r_s}{\sqrt{k}} + \frac{r_s^2}{3k}} \times D_w \quad (9)$$

where  $k = \beta r_f^2(1 - \theta_b)^\gamma$ ,  $S = (1 - \theta_b)[(r_s + r_f)/r_f]^2$ , and  $r_f$  is the radius of keratin microfibril (35 Å). The others are parameters fitted to experimental data:  $\lambda = 1.09$ ,  $\gamma = -1.17$ ,  $\alpha = 9.47$ ,  $\beta = 9.32 \times 10^{-8}$ .

The partition coefficient ( $K_{vw}$ ) in the viable epidermis and dermis is assumed to be the same, and so is the diffusion coefficient ( $D_v$ ,  $\text{m}^2 \text{s}^{-1}$ ), because of the similar multiphase compositions in the two skin layers (20, 31). This approach was also used in other modelling studies (15, 31, 32). We follow the method presented in (15, 20) to relate the partition and

diffusion coefficients to solute ionisation and binding to albumin as follows:

$$K_{vw} = 0.7 \times \left( 0.68 + \frac{0.32}{f_u} + 0.025 f_{non} K_{mw} \right) \quad (10)$$

$$D_v = \frac{10^{-8.15 - 0.655 \log MW}}{0.68 + \frac{0.32}{f_u} + 0.025 f_{non} K_{mw}} \quad (11)$$

where  $f_{non}$  is the non-ionised fraction of solute in the aqueous phase;  $f_{non}$  depends on the chemical dissociation constant and the pH of the solution, and it can be calculated by using the formulate given in (33, p.72) or more sophisticated software tools (*e.g.* ACD/Labs). The fraction of unbound (to albumin) solute ( $f_u$ ) may be estimated by using the QSPR model developed in (34).

Finally, the dermis to blood partition coefficient,  $K_{db}$ , needs to be estimated. In the literature, various QSPR models have been reported for volatile organic compounds, where  $K_{db}$  can be related to experimentally measured oil-to-air and/or saline-to-air partition coefficients (35). Alternatively it can also be estimated by using the Abraham descriptors and accordingly the QSPR model reported in (27).

## Model Demonstration: Clinical Studies of Nicotine

A published clinical study of transdermal delivery of nicotine (23) was used to support model development and demonstration. The model was also applied to predict another clinical study of nicotine (24), which was not considered during model development, to test the prediction performance.

Nicotine replacement therapy has been widely used for the purpose of smoking cessation, and its transdermal delivery has been popular. One important advantage of the transdermal route is that it provides continuous and controlled release of the drug, which has contributed to the reduction of craving and withdrawal symptoms during smoking cessation. As a result, various nicotine transdermal systems have been developed, with many clinical studies reported in the literature (*e.g.*, 23, 36). A brief description of the study by Bannon *et al.* (23), which was used to support model development, is given below.

Bannon *et al.* (23) investigated the absorption of nicotine delivered from a hydrogel based matrix-type transdermal patch (Nicolan™). Three dose levels were studied by varying the surface areas of the patch: 3.5  $\text{cm}^2$  for 15, 7.0  $\text{cm}^2$  for 30, and 14.0  $\text{cm}^2$  for 60 mg. Healthy smokers were recruited for the study, and they agreed to abstain from smoking prior to and during the study which was verified by monitoring the carbon monoxide levels. In the first study, the transdermal patches were applied to the volar forearm of nine subjects for 24 h and the plasma nicotine concentration was measured

at several time points up to 30 h. The aim was to examine the impact of dose level on absorption kinetics. In the multiple dose study, the subjects were given one fresh 30-mg patch every 24 h for 7 days and blood samples were taken at various time points. The total delivered dose was approximately 85% of the nicotine content in the patches, as calculated from measuring the residual nicotine in the patch after removal.

To simulate the above scenarios, various skin physiology and solute physicochemical parameters are needed; these were largely taken from the literature and summarised in Table I. We adjusted the number of cell layers in the stratum corneum according to the reported thickness at volar forearm, which has significant variability within one study and between different studies. The thickness of the stratum corneum was set to 20.5  $\mu\text{m}$ , which is the average measured by Egawa *et al.* (37) (22.6  $\mu\text{m}$ ) and Sandby-Moller *et al.* (38) (18.3  $\mu\text{m}$ ). This thickness corresponds to 23 corneocyte-lipid layers (assuming 0.875  $\mu\text{m}$  for each layer (15)). The thickness of the patch was not given; hence the nicotine concentration in the vehicle has to be estimated. We followed similar modelling studies (*e.g.* 22) to assume a vehicle depth of 100  $\mu\text{m}$ , from which and the given surface area the concentration can be determined.

The partition and diffusion coefficients of nicotine in the hydrogel-based vehicle depend on the properties of the hydrogel. Solute partitioning and diffusion in hydrogel has been widely studied both theoretically and experimentally (39, 40). Hydrodynamic hindrance of hydrogel on the diffusion coefficient is rather limited for small molecules, often less than 10% reduction of that in water (39, 41). For this reason, the

diffusion coefficient of nicotine in the hydrogel vehicle was fixed to the same value as in water (calculated in Eq. (5)). The partition coefficient between hydrogel and water was typically reported to be between 0.5 and 1, depending on the volume fraction of dispersed polymers (40). In this study, the partition coefficient of nicotine between vehicle and water was set to 0.7. Due to the lack of precise information about the vehicle, sensitivity analysis was conducted to investigate the impact of vehicle properties (partition and diffusion coefficients).

The diffusion and partition properties of nicotine in stratum corneum were calculated in the same way as previously verified (14). The fraction of nonionised nicotine at pH 7.4 and binding to plasma protein, which are needed for these calculations, were set to the experimentally reported values:  $f_{non} = 0.31$  and  $f_u = 0.95$  (42, 43). The partition coefficient of nicotine between dermis and blood is also set to the experimental value:  $\log K_{db} = -0.04$  (27). The nicotine clearance in systemic circulation was set to 1.40  $\text{L min}^{-1}$  as reported (43).

The other clinical study reported the systemic kinetics of the Nicorette® Invisi 25 mg Patch™ (McNeil Products Ltd., Maidenhead, UK) (24). The patch was designed to be worn for 16 h and plasma concentration data were available for 32 h. The vehicle concentration was calculated based on the reported loading dose (1.75  $\text{mg/cm}^2$ ), patch size (22.5  $\text{cm}^2$ ) and the assumed vehicle thickness of 100  $\mu\text{m}$ . All other input parameters are the same as the Nicolan case described above. The intention was to further test the prediction performance of the model.

**Table I** The Input Parameters of the Model for Simulating the Nicotine Study

Part name	Parameter	Value
Nicotine	Molecular weight (MW)	162.23 Da
	Octanol-water partition coefficient ( $\log K_{ow}$ )	1.17
	Fraction of non-ionised solute ( $f_{non}$ )	0.31
	Fraction of unbound solute ( $f_u$ )	0.95
Vehicle	Thickness	100 $\mu\text{m}$
	Initial nicotine concentration	428.57 $\text{mg mL}^{-1}$
Stratum corneum	Number of corneocyte layers	23 (volar forearm)
	Width of corneocytes	40 $\mu\text{m}$
	Height of corneocytes	0.8 $\mu\text{m}$
	Thickness of inter-cellular lipid	0.075 $\mu\text{m}$
	The lateral spacing between corneocytes	0.075 $\mu\text{m}$
Viable epidermis	Thickness	100 $\mu\text{m}$
Dermis	Thickness	1200 $\mu\text{m}$
	Dermis-blood partition coefficient of nicotine ( $\log K_{db}$ )	-0.04
Blood	Cardiac output	5.6 $\text{L min}^{-1}$
	Skin blood flow as fraction of cardiac output	5%
	Nicotine clearance in blood (k)	1.40 $\text{L min}^{-1}$

## RESULTS

For the Nicolan patch, the predicted plasma concentration for different dose levels is illustrated in Fig. 2, in comparison with the clinical data. It appears that the model is capable of reproducing the main trend of the kinetics in plasma. This is especially the case for the intermediate dose level of 30 mg. For 60 mg, the model slightly over-predicts the rate of increase in concentration at the beginning, whilst for 15 mg, the peak concentration is slightly over-predicted. It should be noted that in the original report (23), only the mean concentration values of nine subjects were given but not the standard deviation, and thus it is not possible to fully consider the inter-subject variability in comparison. However, for 30 mg, the data from both the single dose study and the first 24 h of the multiple dose study were augmented in Fig. 2, and even these two sets of average data exhibit significant differences. Therefore, the difference between the model prediction and clinical data is well within the variability of such clinical studies.

Table II compares the predicted pharmacokinetic parameters for the single dose study with the experimentally derived data. As observed from Fig. 2, the model tends to predict the time to reach maximum concentration ( $t_{max}$ ) earlier than that indicated by the data, though still within 1.0 ~ 1.5 standard deviation from the average of the data. The prediction of the remaining pharmacokinetic parameters, such as AUCs,  $C_{max}$  and the fraction of absorbed dose ( $f$ ), is in good agreement with the data.

Figure 3 compares the model prediction and clinical data for the 30 mg multiple dose study. Apparently the predicted end-of-day plasma concentration, when the old patch is replaced by a new one, is higher than the actual data. In the collected data, the value at 24 h for the multiple dose study

(4.58 ng mL<sup>-1</sup>) was also reported to be substantially lower than the value for the single dose study (7.90 ng mL<sup>-1</sup>). Therefore the model prediction is in reasonably good agreement with the data. Another observation is that from day 2, the model predicted plasma concentration cycles quite stably with negligible day-to-day variation, whereas the reported clinical data showed variation at 24, 48, 96, 144 and 168 h.

Figure 4 illustrates the simulated disposition of nicotine at different skin layers, in the blood compartment and the cumulative amount cleared from the blood. The simulation was extended to 50 h (*i.e.* 26 h after the patch is removed) to allow for sufficient clearance of nicotine from the system. It can be seen that within the skin, the majority of the applied dose is absorbed in the stratum corneum, whilst the viable epidermis and dermis contain very small proportions. The concentration of nicotine in the stratum corneum is significantly higher than that in the underlying viable epidermis and dermis. There is a large partition coefficient of nicotine between the stratum corneum (lipid) to viable epidermis ( $K = 7.73$ ). The diffusion of nicotine in the viable epidermis and dermis ( $2.36 \times 10^{-10} \text{ m}^2 \text{ s}^{-1}$ ) is also much faster than that in lipid bilayer ( $1.43 \times 10^{-11} \text{ m}^2 \text{ s}^{-1}$ ) and corneocyte ( $2.67 \times 10^{-15} \text{ m}^2 \text{ s}^{-1}$ ) in the stratum corneum. Physiologically, the viable epidermis and dermis contain up to 70% aqueous phase (20), which has important impact on the partition and diffusion coefficients of the lipophilic nicotine. In addition, the concentration of solute in systemic circulation also appears to be much lower than in the stratum corneum, which is likely due to the rapid clearance as a result of metabolism into cotinine (23). The detailed modelling of various plasma clearance pathways, *e.g.* metabolism and transport into other tissues, is outside the scope of this study.

From the simulation results, the relative ratio of nicotine deposition in skin can be obtained. Figure 5 gives the relative percentage nicotine disposition within the stratum corneum; it

**Fig. 2** Comparison of modelling results with the published clinical data of Bannon *et al.* (23) following the application of nicotine transdermal patches with different doses (patch removed after 24 h of application).

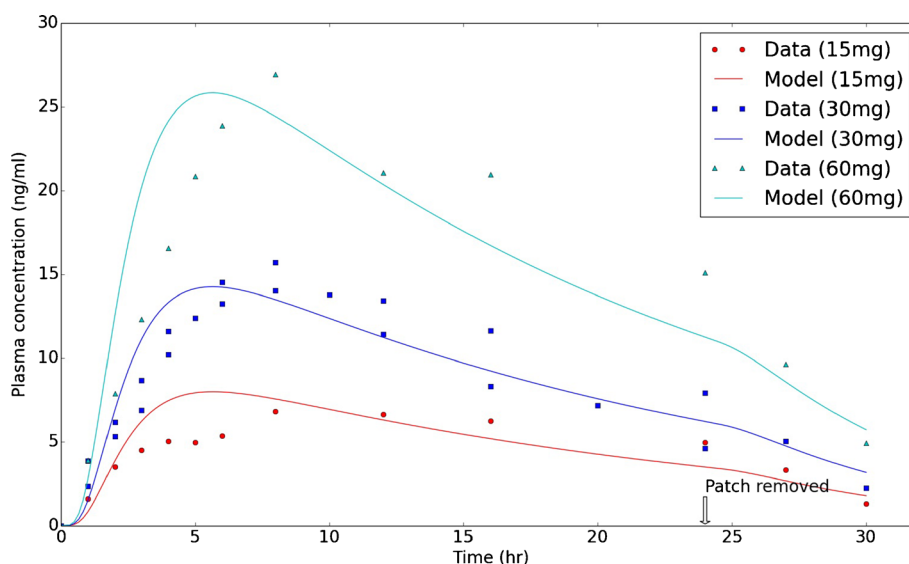


**Table II** Plasma Nicotine Pharmacokinetic Parameters for the Single Dose Study. Standard Deviation is Given in the Parentheses. In the Clinical Study, the Fraction of Solute Absorbed ( $f$ ) was Calculated from Residual Nicotine in the Patch After Removal

Dose level	15 mg Data	Model	30 mg Data	Model	60 mg Data	Model
$AUC_{0-30}$ (ng hr mL <sup>-1</sup> )	152 (34.6)	153	294 (53.1)	273	509 (88.9)	494
$AUC_{inf}$ (ng hr mL <sup>-1</sup> )	170 (36.5)	165	310 (56.4)	294	541 (99.7)	533
$t_{max}$ (hr)	7.78 (4.27)	5.53	7.78 (1.86)	5.53	8.22 (3.07)	5.53
$C_{max}$ (ng mL <sup>-1</sup> )	8.02 (1.96)	8.62	17.1 (5.03)	15.4	28.9 (9.14)	27.9
$f$	0.85 (0.084)	0.82	0.87 (0.024)	0.82	0.83 (0.072)	0.82

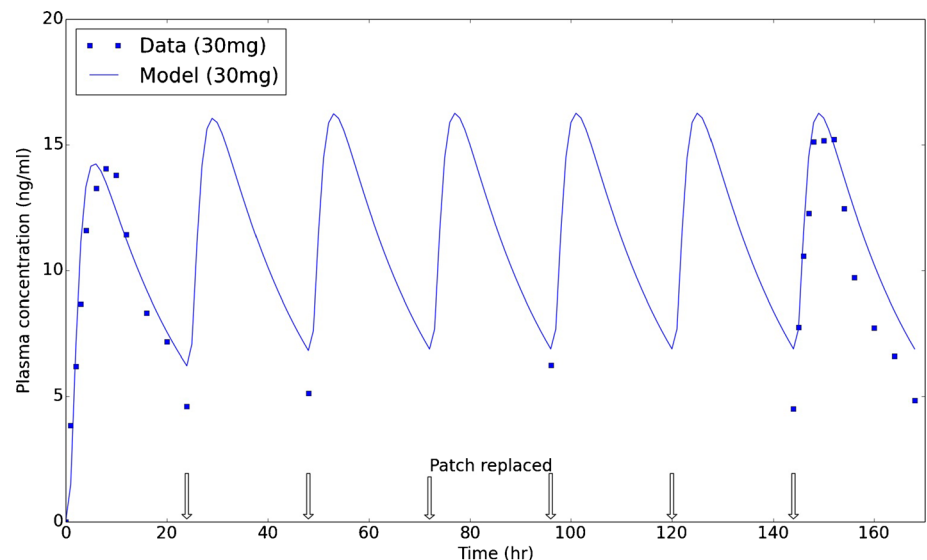
shows that more solute stays in the corneocyte (the “brick”) than in the lipid (the “mortar”). Although the concentration in the lipid is much higher than that in the corneocyte (c.f. Fig. 6), the total volume fraction of lipid in the stratum corneum is only about 8.7% (calculated by using the geometric parameters in Table I), and thus the total solute amount in lipid is less. In addition, the peak amount in the lipid is achieved more quickly than in the corneocyte; this is expected because the diffusion coefficient in the lipid is much higher than that in the corneocyte.

Figure 6 gives detailed disposition of nicotine in the stratum corneum at different time points using two-dimensional concentration surface plots. The profiles vividly illustrate the dominant role of lipid pathway in skin penetration for this lipophilic compound, though the effect of corneocyte is not negligible. At the early stage of permeation, the diffusion along the lipid creates a clear “fingering” effect as seen in the figure. It is also interesting to observe that at the beginning, when solute diffuses along the lipid layer, it may “back-diffuse” from a lower lipid layer to upper corneocytes due to the gradient in chemical potential (considering gradient in concentration and the effect of partitioning). This back-diffusion may slow down the initial penetration rate as corneocytes serve as “reservoirs” and need to be filled with

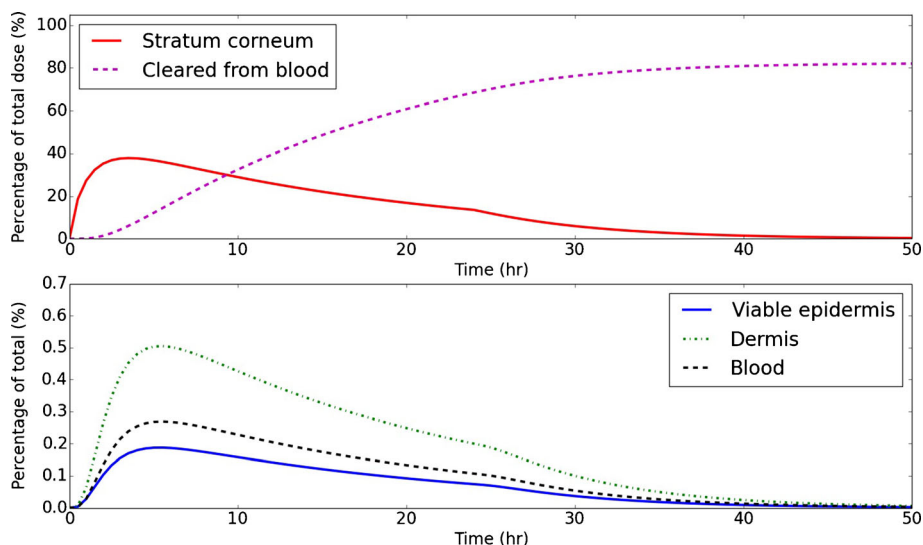
the solute from the lipid. In a later stage, these reservoirs first reach equilibrium with surrounding lipid and then release the solute as the chemical potential in the lipid is further lowered due to diffusion into the dermis and viable dermis. This corresponds to the point when a significant amount of solute has been consumed in the patch. Release from corneocyte reservoirs can be clearly seen when the patch is removed (*i.e.* after 24 h). For example in Fig. 6e and f, the concentration in the centre of the topmost corneocyte layer is even higher than that in the surrounding lipid layer, and when combined with the effect of partitioning the chemical potential gradient creates significant driving force to release the solute.

Figure 7 shows the sensitivity analysis with respect to the model input parameters in the vehicle of the Nicolan study. We first examine the likely effect of varying the partition coefficient between vehicle and water from 1/10 to 10 times of its nominal value ( $K_{vw} = 0.7$ ). Increasing the partition coefficient represents the use of a more hydrophobic vehicle formulation. Conversely, decreasing the partition coefficient mimics the use of a more hydrophilic formulation. Clearly, changing vehicle partition property has a significant impact on the delivered plasma concentration (Fig. 7a). Using a more hydrophilic vehicle of lower partition coefficient results in faster increase of plasma concentration, shorter  $t_{max}$ , and higher

**Fig. 3** Comparison of modelling results with clinical data of Bannon *et al.* (23) following the application of nicotine transdermal patches that were replaced every 24 h.



**Fig. 4** Simulated disposition of nicotine in different skin layers and the circulation. The patch is removed after 24 h of application.



$C_{\max}$  of nicotine. The plasma concentration of nicotine at later stage is also more rapidly depleted. In contrast, by using a more hydrophobic vehicle of higher partition coefficient, nicotine is predicted to favour staying in the vehicle, leading to sustained slower release into skin and blood circulation. For a given vehicle formulation, different solutes also have different vehicle:water partition coefficients but the effect is more complicated, as the partition and diffusion properties in the skin will also vary.

We also examine the effect of nicotine mobility in the vehicle. The diffusion coefficient of nicotine in vehicle was reduced to 1/10, 1/100, 1/1000 and 1/10000. This essentially models the effect of controlled releases. Figure 7b shows that reducing the diffusion coefficient of the vehicle by two orders of magnitude has negligible impact on the pharmacokinetics of nicotine delivery – its plasma concentration appears to be

not distinguishable. The diffusivity of nicotine in vehicle only starts to reduce the plasma concentration when this parameter is reduced by more than 100-fold. Further reduction of the diffusion in vehicle makes this parameter comparable with that in skin, and thus it slows down the penetration, leading to sustained slow release and lower plasma concentration.

Finally, Fig. 8 illustrates the results for the separate Nicorette data set reported by DeVeauh-Geiss *et al.* (24). Good agreement between model prediction and clinical data is also achieved. The predicted kinetics is appreciably faster than the actual data (experimentally derived  $t_{\max}$  is 12.0 h, while the prediction gives 6.0 h). Nevertheless, the model was able to describe the main pattern of the profile, with good prediction of  $AUC_{0-32}$  (model: 262.9 ng hr mL<sup>-1</sup>; data: 238.51 ng hr mL<sup>-1</sup>) and  $C_{\max}$  (model: 14.50 ng mL<sup>-1</sup>; data: 16.56 ng mL<sup>-1</sup>).

**Fig. 5** Simulated disposition of nicotine in lipid and corneocytes, and their relative amount (percentage) with respect to the total nicotine in the stratum corneum. The initial dose in the vehicle is 30 mg, and the patch is removed after 24 h of application.

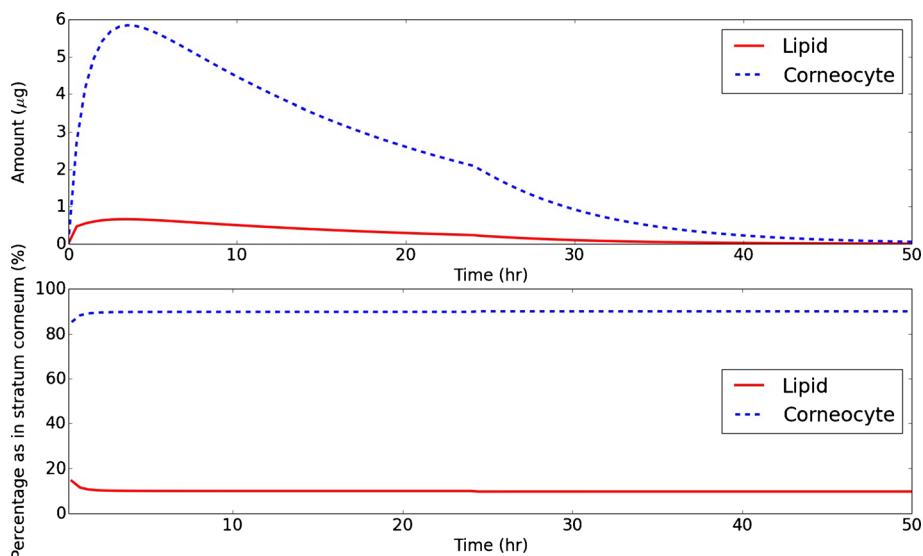
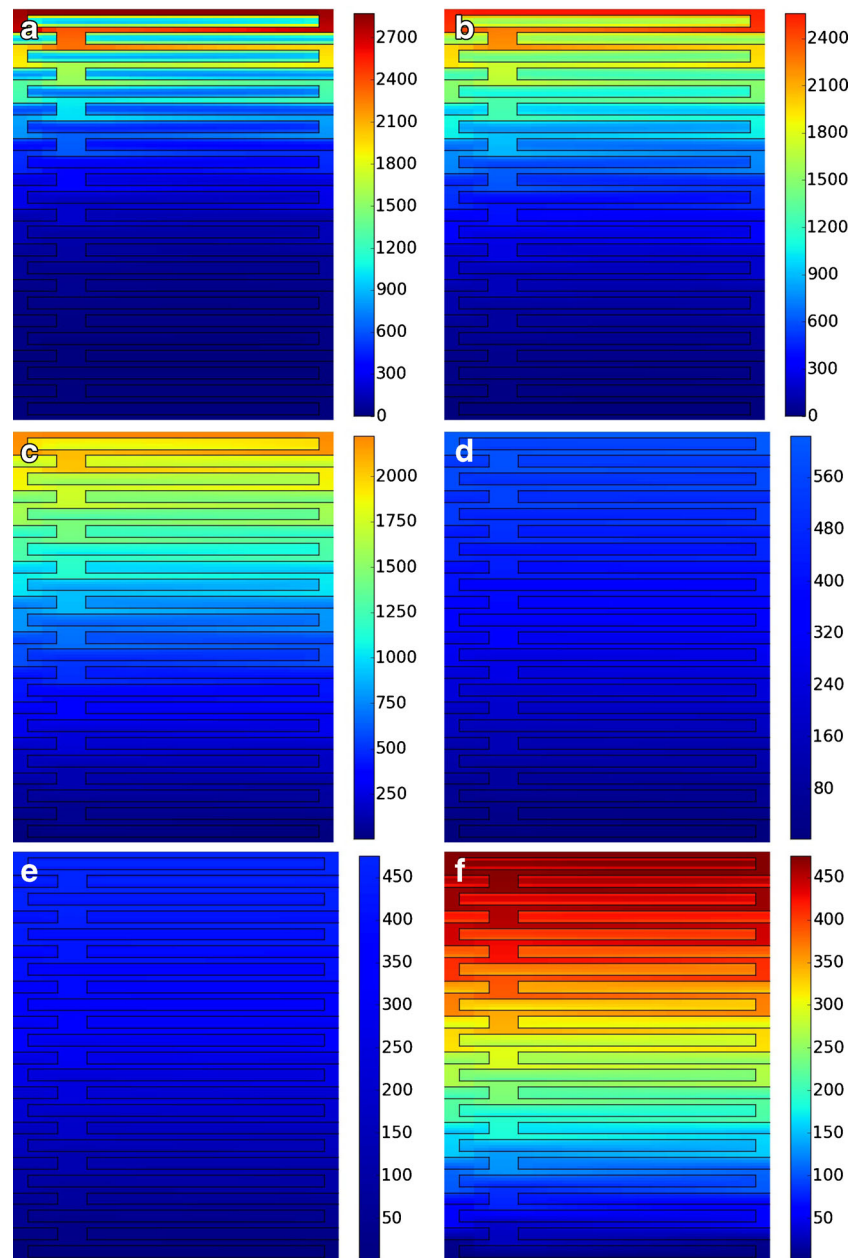


**Fig. 6** Microscopic disposition of nicotine in the stratum corneum. The initial dose in the vehicle is 30 mg, and the patch is removed after 24 h of application. The unit in all colour maps is mg mL<sup>-1</sup>. The boundary between lipid and corneocytes are marked with solid line. Note that because of the very small lipid size relative to that of corneocytes, the 2D simulation domain is illustrated in terms of grid points and thus is not to scale. **(a)** 0.5 h; **(b)** 1 h; **(c)** 2 h **(d)** 24 h; **(e)** 25 h; **(f)** 25 h with adjusted colour map. The same, fixed colour map was used for **(a)**–**(e)**, but to illustrate the detailed concentration profile at 25 h, the colour map in **(e)** was adjusted to produce **(f)**.



## DISCUSSIONS

The primary intention of this paper is to present an integrated mechanistic model that captures the important molecular and microscopic principles involved in skin penetration and systemic bioavailability. To demonstrate the use of the integrative mechanistic model, two sets of published clinical data of nicotine patches (23, 24) have been simulated. The predicted nicotine concentration in systemic circulation is in good agreement with the reported clinical data. Furthermore, after validation with plasma concentration, such a bottom-up model can predict the microscopic kinetic and bioavailability information in various skin layers, which may not be easily

measured in clinical studies but are of particular importance for intended topical delivery. From the simulation, the disposition of nicotine in different skin layers is also obtained (Figs. 4, 5 and 6).

In the simulation, all input parameters for the vehicle, stratum corneum, viable dermis, dermis and systemic circulation were derived separately from their molecular, microscopic and physiology bases. The nicotine partition and diffusion coefficients in the hydrogel-based vehicle were estimated by referring to “typical” hydrogel properties and the impact on solute diffusion/partition reported in the literature (39, 40). Reducing the diffusion coefficient in vehicle within 3 orders of magnitude was found to have negligible impact on the

**Fig. 7** Sensitivity analysis of the impact of vehicle properties on systemic kinetics of nicotine. **(a)** The impact of vehicle:water partition coefficient; **(b)** The impact of diffusion coefficient in vehicle. The legend “ $\times 0.1$ ” denotes that the input parameter in the base model was multiplied by 0.1 to obtain the result. Experimental data is from Bannon *et al.* (23).

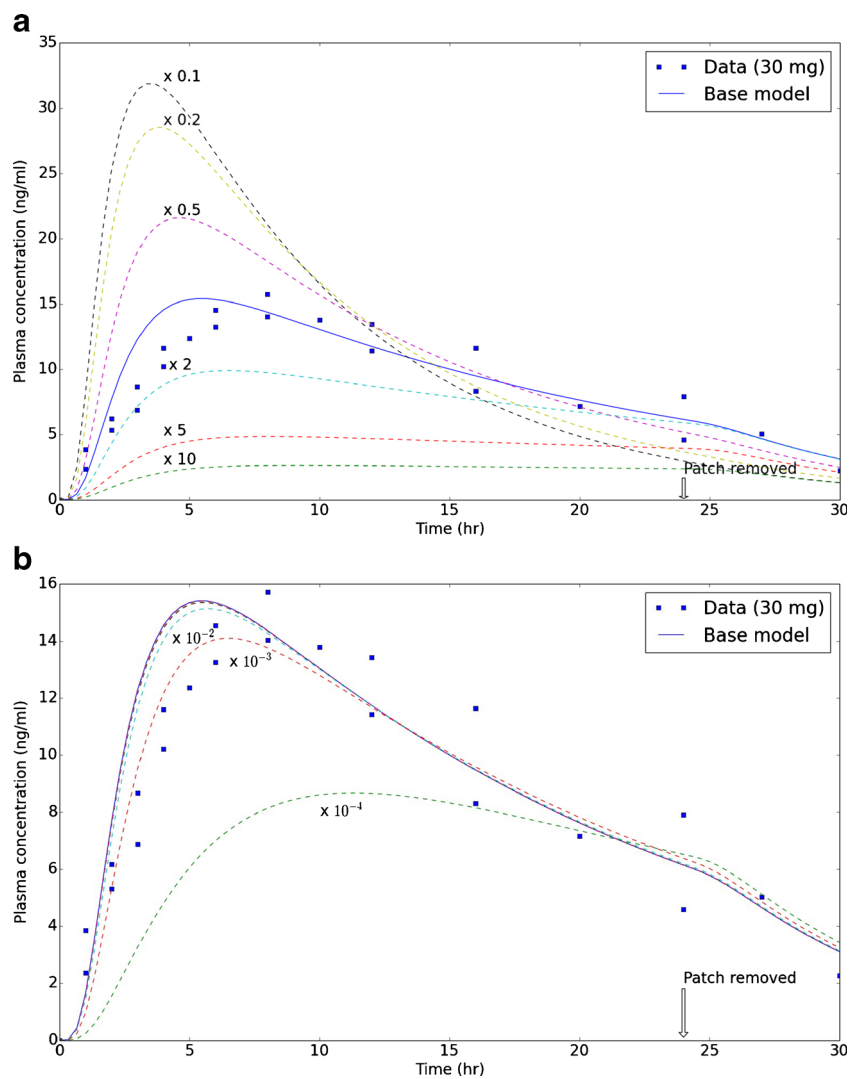
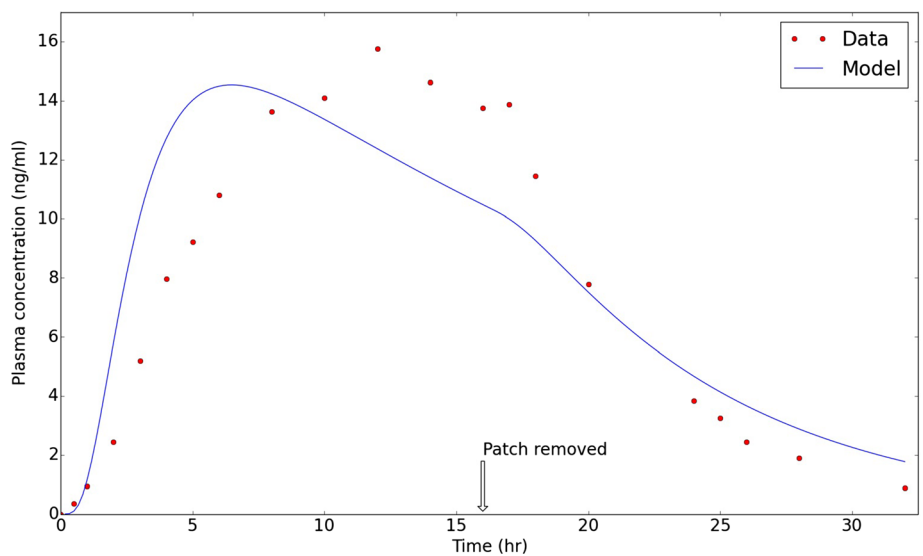


**Fig. 8** Comparison of model prediction with the published clinical data of Nicorette patch from DeVaugh-Geiss *et al.* (24).



simulation results. The partition coefficient between vehicle and water however does have a significant effect. The chosen value (0.7) was derived by mainly considering the exclusion effect. Mathematically, vehicle partition coefficient can be further refined by optimisation so that the fit to the clinical data could be further improved. Nevertheless, that vehicle partition coefficient has significant effect on the simulation results, as shown in the sensitivity analysis, is a valuable insight for controlling the delivery of topically applied nicotine. Experimental and theoretical insight for designing vehicle partition property is an area of active research (39–41). Here we performed a systematic sensitivity analysis of the vehicle. Increasing the hydrophobicity of the vehicle leads to slower release and sustained delivery of nicotine to systemic circulation. Using more hydrophilic vehicle formulation leads to faster delivery depletion of nicotine in the plasma circulation. Reducing the diffusion coefficient of the vehicle by 3 orders of magnitude has negligible effect on the pharmacokinetics of nicotine release, absorption and bioavailability. For controlled release formulations to be effective, the equivalent diffusion coefficient of nicotine in the vehicle has to be reduced by more than two orders of magnitude.

In the clinical studies only the area of the patch is given, but not the depth. For the simulation, the thickness of the vehicle is estimated from the dose. Varying the depth of the vehicle requires the corresponding adjustment of nicotine concentration and hence can impact on pharmacokinetics of plasma concentration of nicotine but the shape of curve will remain. This feature enabled us to estimate the thickness of the vehicle to be ca. 100  $\mu\text{m}$ . The corresponding initial nicotine concentration in the vehicle (Nicolan) is 428.57  $\text{mg mL}^{-1}$ , or 42.67% w/w, (assuming the vehicle as an ideal aqueous solution). This value is close to the nicotine concentration (48% w/w) achieved for the maximum steady-state flux across skin (44).

## CONCLUSION

This paper reports the development of a detailed mechanistic model that integrates the skin penetration model with systemic circulation kinetics. To validate the model, the published clinical data of transdermal pharmacokinetics of nicotine was simulated. All input parameters for the model, including the solute (nicotine), the vehicle, the stratum corneum, the dermis, the viable dermis and systemic circulation, were determined independent of the *in vivo* pharmacokinetics being predicted. The integrated mechanistic modelling has significantly extended the applicability of the current microscopic skin penetration model by providing prediction of solute concentration in the blood. In addition, by using advanced computational techniques, we report the simulation of detailed two-dimensional concentration profile in the stratum corneum, which provides useful information of the local sub-cellular

disposition kinetics in skin. The future work will be focused on more comprehensive validation of the model with a wide range of chemicals, and further assessment of the usability of this model in the design and safety assessment of pharmaceutical, personal care and other chemical products to which the transdermal route is relevant.

## ACKNOWLEDGMENTS AND DISCLOSURES

This work was supported by the UK Royal Academy of Engineering (grant number: ISS1415\7\46), the Biotechnology and Biological Sciences Research Council (grant number: BB/L502042/1), and Unilever Research Colworth, UK. We would like to thank Drs Stephen Glavin and Ian Sorrell at the Safety and Environmental Assurance Centre, Unilever, for useful discussions on dermal pharmacokinetic modelling and safety assessment.

## REFERENCES

- Mitragotri S. Modeling skin permeability to hydrophilic and hydrophobic solutes based on four permeation pathways. *J Control Release*. 2003;86:69–92.
- Rush AK, Miller MA, Smith III ED, Kasting GB. A quantitative radioluminographic imaging method for evaluating lateral diffusion rates in skin. *J Control Release*. 2015;216:1–8.
- Potts RO, Guy RH. Predicting skin permeability. *Pharm Res*. 1992;9:663–9.
- Yamashita F, Hashida M. Mechanistic and empirical modeling of skin penetration of drugs. *Adv Drug Deliv Rev*. 2003;55:1185–99.
- Bookout Jr RJ, McDaniel CR, Quinn DW, McDougal JN. Multilayered dermal subcompartments for modelling chemical absorption. *SAR QSAR Environ Res*. 1996;5:133–50.
- Liu X, Grice JE, Lademann J, Otberg N, Trauer S, Patzelt A, *et al*. Hair follicles contribute significantly to penetration through human skin only at times soon after application as a solvent deposited solid in man. *Br J Clin Pharmacol*. 2012;72:768–74.
- Anissimov YG, Jepps OG, Dancik Y, Roberts MS. Mathematical and pharmacokinetic modelling of epidermal and dermal transport processes. *Adv Drug Deliv Rev*. 2013;65:169–90.
- Anissimov YG, Roberts MS. Diffusion modeling of percutaneous absorption kinetics: 1. Effects of flow rate, receptor sampling rate and viable epidermal resistance for a constant donor concentration. *J Pharm Sci*. 1999;88:1201–9.
- Kasting GB. Kinetics of finite dose absorption through skin 1. Vanillylnonanamide. *J Pharm Sci*. 2001;90:202–12.
- Hansen S, Henning A, Naegel A, Heisig M, Wittum G, Neumann D, *et al*. In-silico model of skin penetration based on experimentally determined input parameters. Part I: experimental determination of partition and diffusion coefficients. *Eur J Pharm Biopharm*. 2008;68:352–67.
- Wang TF, Kasting GB, Nitsche JM. A multiphase microscopic diffusion model for stratum corneum permeability. I. Formulation, solution, and illustrative results for representative compounds. *J Pharm Sci*. 2006;95:620–48.
- Wang TF, Kasting GB, Nitsche JM. A multiphase microscopic diffusion model for stratum corneum permeability. II. Estimation of physicochemical parameters and application to a large permeability database. *J Pharm Sci*. 2007;96:3024–51.

13. Chen L, Lian G, Han L. Use of “bricks and mortar” model to predict transdermal permeation: model development and initial validation. *Ind Eng Chem Res.* 2008;47:6465–72.
14. Chen L, Lian G, Han L. Modeling transdermal permeation. Part I. Predicting skin permeability of both hydrophobic and hydrophilic solutes. *AIChE J.* 2010;56:1136–46.
15. Chen L, Han L, Saib O, Lian G. In silico prediction of percutaneous absorption and disposition kinetics of chemicals. *Pharm Res.* 2015;32:1779–93.
16. Frasch HF, Barbero AM. Application of numerical methods for diffusion-based modelling of skin permeation. *Adv Drug Deliv Rev.* 2013;65:208–20.
17. Jepps OG, Dancik Y, Anissimov YG, Roberts MS. Modeling the human skin barrier—towards a better understanding of dermal absorption. *Adv Drug Deliv Rev.* 2013;65:152–68.
18. Anissimov YG, Roberts MS. Modelling dermal drug distribution after topical application in human. *Pharm Res.* 2011;28:2119–29.
19. Kretsos K, Kasting GB. A geometric model of dermal capillary clearance. *Math Biosci.* 2007;208:430–53.
20. Kretsos K, Miller MA, Zamora-Estrada G, Kasting GB. Partitioning, diffusivity and clearance of skin permeants in mammalian dermis. *Int J Pharm.* 2008;346:64–79.
21. Ibrahim R, Nitsche JM, Kasting GB. Dermal clearance model for epidermal bioavailability calculations. *J Pharm Sci.* 2012;101:2094–108.
22. Polak S, Ghobadi C, Mishra H, Ahmadi M, Patel N, Jamei M, *et al.* Prediction of concentration-time profile and its inter-individual variability following the dermal drug absorption. *J Pharm Sci.* 2012;101:2584–95.
23. Bannon YB, Corish J, Corrigan OI, Devane JG, Kavanagh M, Mulligan S. Transdermal delivery of nicotine in normal human volunteers: a single dose and multiple dose study. *Eur J Clin Pharmacol.* 1989;37:285–90.
24. DeVaugh-Geiss AM, Chen LH, Kotler ML, Ramsay LR, Durcan MJ. Pharmacokinetic comparison of two nicotine transdermal systems, a 21-mg/24-hour patch and a 25-mg/16-hour patch: a randomized, open-label, single-dose, two-way crossover study in adult smokers. *Clin Ther.* 2010;32:1140–8.
25. Guyton AC, Hall JE. *Textbook of medical physiology.* 11th ed. Philadelphia: Elsevier; 2006.
26. Hindmarsh AC, Brown PN, Grant KE, Lee SL, Serban R, Shumaker DE. SUNDIALS: suite of nonlinear and differential/algebraic equation solvers. *ACM Trans Math Softw.* 2005;31:363–96.
27. Abrham MH, Ibrahim A. Blood or plasma to skin distribution of drugs: a linear free energy analysis. *Int J Pharm.* 2007;329:129–34.
28. Mitragotri S, Johnson ME, Blankschtein D, Langer R. An analysis of the size selectivity of solute partitioning, diffusion, and permeation across lipid bilayers. *Biophys J.* 1999;77:1268–83.
29. Nitsche JM, Wang TF, Kasting GB. A two-phase analysis of solute partitioning into the stratum corneum. *J Pharm Sci.* 2006;95:649–66.
30. Wang LM, Chen LJ, Lian GP, Han LJ. Determination of partition and binding properties of solutes to stratum corneum. *Int J Pharm.* 2010;398:114–22.
31. Dancik Y, Miller MA, Jaworska J, Kasting GB. Design and performance of a spreadsheet-based model for estimating bioavailability of chemicals from dermal exposure. *Adv Drug Delivery Rev.* 2013;65:221–36.
32. Kasting GB, Miller MA, Nitsche JM. Absorption and evaporation of volatile compounds applied to skin. In: Waltersand KA, Roberts MS, editors. *Dermatologic, cosmeceutic, and cosmetic development.* Boca Raton: CRC Press; 2007. p. 385–99.
33. Florence AT, Attwood D. *Physicochemical principles of pharmacy.* 5th ed. London: Pharmaceutical Press; 2011.
34. Yamazaki K, Kanaoka M. Computational prediction of the plasma protein-binding percent of diverse pharmaceutical compounds. *J Pharm Sci.* 2004;93:1480–94.
35. Meulenberg CJW, Vijverberg HPM. Empirical relations predicting human and rat tissue:air partition coefficients of volatile organic compounds. *Toxicol Appl Pharmacol.* 2000;165:206–16.
36. Sobue S, Sekiguchi K, Kikkawa H, Irie S. Effect of application sites and multiple doses on nicotine pharmacokinetics in healthy male Japanese smokers following application of the transdermal nicotine patch. *J Clin Pharmacol.* 2005;45:1391–9.
37. Egawa M, Hirao T, Takahashi M. *In vivo* estimation of stratum corneum thickness from water concentration profiles obtained with Raman spectroscopy. *Acta Derm Venereol.* 2007;87:4–8.
38. Sandby-Møller J, Poulsen T, Wulf HC. Epidermal thickness at different body sites: relationship to age, gender, pigmentation, blood content, skin type and smoking habits. *Acta Derm Venereol.* 2003;83:410–3.
39. Amsden B. Solute diffusion within hydrogels. Mechanisms and models. *Macromolecules.* 1998;31:8382–95.
40. Dursch TJ, Taylor NO, Liu DE, Wu RY, Prausnitz JM, Radke CJ. Water-soluble drug partitioning and adsorption in HEMA/MAA hydrogels. *Biomaterials.* 2014;35:620–9.
41. Phillips RJ. A hydrodynamic model for hindered diffusion of proteins and micelles in hydrogels. *Biophys J.* 2000;79:3350–3.
42. Benowitz NL, Jacob III P, Jones RT, Rosenberg J. Interindividual variability in the metabolism and cardiovascular effects of nicotine in man. *J Pharmacol Exp Ther.* 1982;221:368–72.
43. Benowitz NL, Hukkanen J, Jacob III P. Nicotine chemistry, metabolism, kinetics and biomarkers. *Handb Exp Pharmacol.* 2009;192:29–60.
44. Kuswahyuning R, Roberts MS. Concentration dependency in nicotine skin penetration flux from aqueous solutions reflects vehicle induced changes in nicotine stratum corneum retention. *Pharm Res.* 2014;31:1501–11.